Chromatin bound by survivin regulates the glycolytic switch in interferon-γ producing CD4$^+$ T cells

Malin Erlandsson (malin.erlandsson@rheuma.gu.se)
University of Gothenburg https://orcid.org/0000-0003-1100-7577
Karin Andersson
Medicine https://orcid.org/0000-0002-9475-3040
Nina Oparina
University of Gothenburg
Venkataragavan Chandrasekaran
University of Gothenburg
Anastasios Damdimopoulos
Karolinska Institute
Maria-Jose Garcia-Bonete
University of Gothenburg https://orcid.org/0000-0002-8832-4338
Zakaria Einbeigi
Sahlgrenska Academy and University Hospital
Sofia Silfverswärd
University of Gothenburg https://orcid.org/0000-0002-6641-2759
Marcela Pekna
University of Gothenburg https://orcid.org/0000-0003-2734-8237
Gergely Katona
University of Gothenburg https://orcid.org/0000-0002-2031-8716
Maria Bokarewa
University of Gothenburg https://orcid.org/0000-0001-9424-5145

Article

Keywords: metabolism, transcriptional regulation, survivin/BIRC5, T cells, interferon-gamma, IRF1, SMAD3

Posted Date: December 28th, 2021

DOI: https://doi.org/10.21203/rs.3.rs-1148712/v1

Abstract

Upon activation, $CD4^+$ T cells adapt metabolically to fulfill their effector function in autoimmunity. Here we show that nuclear survivin is essential for transcriptional regulation of glucose utilization. We found that the glycolytic switch in interferon (IFN) g–producing $CD4^+$ cells is dependent on a complex of survivin with interferon regulatory factor 1 (IRF1), and Smad3 and was reversed by survivin inhibition. Transcriptome analysis of $CD4^+$ cells and sequencing of survivin-bound chromatin identified a hub of metabolism regulating genes whose transcription depended on survivin. Direct binding of survivin to IRF1 and SMAD3 promoted IRF1-mediated transcription, repressed SMAD3 activity, and lowered *PFKFB3* production. Inhibiting survivin upregulated *PFKFB3*, restored glycolysis, and reduced glucose uptake, improving control over IFNg-dependent T-cell functions. Thus, IRF1-survivin-SMAD3 interactions are important for metabolic adaptation of $CD4^+$ cells and provide an attractive strategy to counteract IFNg-dependent inflammation.

Introduction

Activated $CD4^+$ effector T cells are key players in autoimmune inflammation. These cells migrate, proliferate, and produce signal molecules at sites of inflammation to mobilize immunity. Upon activation, $CD4^+$ cells metabolize glucose via the pentose phosphate pathway rather than the tricarboxylic acid (TCA) cycle[1]—a change reflected in the remarkable shift of energy production and biosynthetic pathways that fuel effector responses[2,3]. The increase in glucose consumption sustains the increased energy demands and facilitates production of IFNg[4,5]—the principal coordinator of adaptive immune responses in chronic inflammation. Shared IFNg-dependent processes are central for the pathogenesis of autoimmune diseases[4,6], but the exact mechanism connecting glucose metabolism with IFNg production remains unclear. Strategies to interfere with these processes by targeting concordant changes in the expression of IFN-sensitive genes in blood leukocytes and target tissues may have broad therapeutic potential for autoimmune disorders. Inhibition of anabolic adaptation, which fuels IFNg production, is an appealing approach to reduce the effects of IFNg in autoimmunity.

Survivin, an oncoprotein encoded by *BIRC5* and widely expressed in solid and hematological malignancies, is essential for renewal of nonmalignant cells[7,8] and may help regulate gene expression[7,9-11]. It is also essential for T-cell development. Conditional deletion of survivin in thymocytes reduces mature $CD4^+$ and $CD8^+$ T cell populations[12] and leads to dysfunctional T-cell receptors and inability to mount a proper immune response to an antigen challenge[13]. Survivin expression declines in mature T cells, but re-appears during critical phases of phenotype transition, such as the effector phenotype acquisition by $CD4^+$ or $CD8^+$ memory T cells[14]. Survivin is associated with increased severity and flare-up of autoimmune conditions, including arthritis[15], psoriasis, and multiple sclerosis[16]. Targeting survivin in experimental and clinical autoimmunity efficiently reduces inflammation, proliferation, and tissue damage[17-21]. However, the role of survivin in cell metabolism has not been investigated.

In this study, we explored the role of nuclear survivin in maintaining the effector phenotype in IFNg-producing Th1 cells acting through the transcriptional control of glucose utilization. To study this, we performed a genome-wide deep sequencing of the survivin precipitated chromatin regions; identified survivin interactors on chromatin, and the biological processes regulated by survivin in cooperation with the identified interactors. Combining chromatin and transcriptome analyses with functional studies we searched for the genes sensitive to survivin inhibition and proposed a novel survivin-dependent mechanism coordinating metabolic adaptations during activation of $CD4^+$ T cells in autoimmunity.

Results

Survivin is an essential marker of the IFNg-producing cells phenotype. Flow-cytometry analysis of $CD4^+$ cells from the blood of 22 patients with rheumatoid arthritis (RA) showed that the effector cells (T_{EFF}, $CD62L^{neg}CD45RA^{+/-}CD27^{neg}$) had higher levels of survivin than memory cells; 5.4–16.4% (mean 9.2%) of T_{EFF} cells contained survivin and had highest amount of survivin per cell (Fig. 1a). The phenotype of survivin-producing T_{EFF} cells was determined by RNA-seq analysis of $CD4^+$ cells. Unsupervised clustering of the samples by the core genes characteristic of T-helper subsets[22] identified accumulation of survivin/*BIRC5* in the T_{EFF} cluster marked by expression of Th1 signature genes (*e.g.*, *TBX21, EOMES, IL2RA,* and *IFNG*) (Fig. 1b and Supplementary Fig. 1a) and cytokines (IFNg, IL9, IL10, and IL13) (Fig. 1d), which correlated with *BIRC5* expression (Supplementary Fig. 1b). Comparison of $BIRC5^{hi}$ and $BIRC5^{lo}$ $CD4^+$ cells revealed the complete Th1 signature enriched in $BIRC5^{hi}$ cells (Fig. 1d).

Availability and efficient metabolism of glucose are required for IFNg production and effector function of Th1 cells. Expression of the main glucose metabolism regulators HIF-1a and the catalytic subunit of AMPK-associated kinase (*PRKAA1*) differed between $BIRC5^{hi}$ and $BIRC5^{lo}$ $CD4^+$ cells, but their expression of *MYC* and *MTOR* was similar (Fig. 1e). Since *HIF1A* expression is controlled by hypoxia, the selective enrichment in *HIF1A* prompted us to evaluate other genes of the hypoxia signature[23]. We found that $BIRC5^{hi}$ cells overexpress the canonical HIF-1a target genes, including lactate dehydrogenase (*LDHA*), enolase (*ENO1*), phosphoglycerate kinase 1 (*PGK1*), and aldolase A (*ALDOA*), corrrelated with glucose metabolism (Supplementary Fig. 1c). Specifically, $BIRC5^{hi}$ cells were deficient in the key regulator of glucose processing, *PFKFB3* (Fig. 1e). As a result, glucose was shunted to the pentose phosphate pathway, as shown by increased expression of glucose-6-phosphate dehydrogenase (*G6PD*) and 6-phosphogluconolactonate (*PGLS*) and by increased expression of ATP citrate lyase (*ACLY*), indicating increased fatty acid metabolism. The correlation matrix of the core set of Th1 genes and glycolysis markers revealed clear distinctions in biological processes between $BIRC5^{hi}$ and $BIRC5^{lo}$ cells (Fig. 1f). The tight interactions in $BIRC5^{hi}$ cells suggested that survivin expression is functionally connected to these processes.

Survivin-bound chromatin is predicted to regulate carbohydrate metabolism

Since survivin has been reported to bind to genomic DNA elements that regulates gene transcription[9-11], we investigate survivin-bound chromatin on the whole-genome level. Chromatin immunoprecipitation sequence (ChIP-seq) analysis of 12 $CD4^+$ cell cultures pooled in 4 replicates (Fig. 2a) revealed 13,704 nonredundant survivin-ChIP peaks (enrichment against input, adjusted $p < 10^{-5}$). The peaks were unevenly distributed across the genome and were specifically enriched in a region within 10–100 kb of the regulatory chromatin area occupied by promoters, enhancers, chromatin insulator regions, and CTCF binding sites (Fig. 2b, c).

To characterize the TF landscape of the survivin-ChIP peaks, we used the global ChIP-seq dataset for 1034 human transcriptional regulators in the ReMap database[24] to annotate the set of nonredundant survivin-ChIP peaks. We identified 146 TF candidates that were significantly enriched across the survivin-ChIP peaks with 0 kb (minimal threshold for the overlapping peaks 10%) and 100-kb flanking regions (Fig. 2d) and compared them to regions within 1 Mb of the peaks. The TF candidates identified by this approach were tightly associated (Fig. 2d). The q significance of association with survivin was higher for TFs in the regions of 0 to 100 kb and lower for TFs within 1Mb.

To identify TFs in open chromatin of $CD4^+$ cells, we used the ATAC-seq dataset (GSE138767[24]) to annotate nonredundant survivin-ChIP peaks. Survivin was tightly associated with a subset of TFs comparable to those identified by whole-genome analysis (Fig. 2d, inset). The q significance of the association did not change between the chromatin regions accessible at 2 and 4 h. The top TFs identified by both analyses were those regulating glucose and insulin metabolism, including CREBBP, KDM5B, DDX5, FOXK2, CTBP1, and IKZF1.

To identify biological processes regulated by chromatin-bound survivin, we analyzed the functions of the 146 TFs that co-localized with survivin peaks (Fig. 2e) and 2749 protein-coding genes expressed in $CD4^+$ cells (RNA-seq, normalized raw counts >0.5) and used Gene Ontology terms to annotate them to the survivn peaks (Supplementary Fig. 2a). This approach identified functional groups that regulate chromatin, protein modification, and metabolism (Fig. 2e). Other functional groups regulated the response to hypoxia and organic substances, including glucose (Fig. 2e and Supplementary Table 1). In agreement with the functional annotation of TFs, gene set enrichment analysis of the protein-coding genes expressed in $CD4^+$ cells and annotated to the survivin peaks revealed significant enrichment in processes regulating cellular biogenesis, carbohydrate metabolism, and hydrolase activity (Supplementary Fig. 2b).

Thus, survivin is frequently located near *cis*-regulatory elements (REs) and is functionally linked to regulation of protein and carbohydrate metabolism.

Survivin restricts *PFKFB3* expression and changes the metabolic requirements of $CD4^+$ cells. To investigate the role of survivin in the predicted biological processes, we used YM155 to inhibit survivin function[10,25] in freshly isolated $CD4^+$T cells using YM155. Cells were polarized with IFNg for the final 2 h. Comparison of differentially expressed genes (DEGs) identified by RNA-seq analysis of YM155-treated (0

and 10 nM) $CD4^+$ cells (nominal $p < 0.05$, DESeq2) with those annotated to survivin peaks showed that 11.8% (24 h) and 4.5% (72 h) of the protein-coding genes expressed in $CD4^+$ cells were sensitive to survivin inhibition (Fig. 3a). Using the curated TRRUST database of gene regulatory relationships, we identified the central metabolism regulators HIF-1a, c-MYC, and SP1 as the upstream transcriptional supervisors of the DEGs after 24 h and 72 h of survivin inhibition. Other effects were attributed to the activity of SMAD4, JUN, NF-kB, RELA, ETS1 TFs at 24 h and to interferon regulatory factor 1 (IRF1) and the MHC class II transactivator at 72 h (Fig. 3b).

To study in detail the enzymes involved in cellular glucose utilization (Fig. 3c), we analyzed YM155-treated and IFNg-polarized $CD4^+$ cells by RNA-seq. We found that mRNA levels of *PFKFB3* and *LDHA* increased rapidly, promoting conversion of pyruvate into lactate, and that *PGLS* and *ACLY* mRNA levels decreased, indicating downregulation of the pentose phosphate pathway and fatty acid metabolism (Fig. 3d). These effects of survivin inhibition blocked the alterations in carbohydrate metabolism seen in the $BIRC5^{hi}$ $CD4^+$ cells from RA patients (Fig. 1f) but did not alter the mRNA levels of *HIF1A* or its metabolic targets *HK2*, *ALDOA*, *ENO1*, and *GAPDH*.

To assess the role of survivin in regulating glucose uptake by $CD4^+$ cells, we measured the accumulation of glucose labeled with the fluorescent dye D-glucose derivate 2-N-nitrobenz-2-oxa-1,3diazol-4-amino]-2 deoxy-D-glucose (2NBD) in $CD4^+$ cells activated with aCD3/IFNg. YM155 reduced uptake of 2NBD-glucose (Fig. 3e), resulting in decreased expression of the HIF-1a-controlled sugar transporters GLUT1 (encoded by *SLC2A1*), glucose-6-phosphate translocase (*SLC37A4*), and proton-associated sugar transporter A (*SLC45A1*) and the hypoxia-sensing proteins SESN2, PYHIN1, and NLRX1 (Fig. 4a). Survivin inhibition also activated expression of (1) the sugar sensors CDK5R1, KLF10, IL21R, and RXRA, (2) the transporters of neutral amino acids SLC7A5, and (3) the transporter of glutamate SLC1A4 controlled by c-Myc (Fig. 3g).

Survivin inhibition resets TGF-beta/SMAD signaling and promotes phenotype transition in $CD4^+$T cells. The reset of PFKFB3-dependent glucose metabolism reduced IFNg production by $CD4^+$ cells treated with YM155 for 24 h and 72 h (Fig. 4a) and inhibited IFN-dependent processes (Supplementary Fig. 2c). After 24 h, canonical IFN-sensitive genes were repressed, including cytotoxic *PRF1* and *GNL1*, the proinflammatory cytokines *CXCL8* and *IL1b*, and receptors that promote clonal T-cell expansion (*IL2RA, SLAMF7*, *IL10RA)* and joint homing (*CX3CR1, ITGB3, ICAM2, TREM25)* (Fig. 4b). The downregulation of IFN-sensitive genes was even more pronounced after 72 h and involved multiple IRF1-dependent genes (*e.g.*, *SOCS1* and *HLA* family genes). Importantly, the IFN-sensitive genes included in autoimmunity signatures of RA[26], systemic lupus erythematosus [27] and Sjögren's syndrome[28] (*e.g.*, *IRF7, GAS6, IFI35, IFITM2, ISG15, ISG20, ODF3B*) were also downregulated. (Fig. 4c).

The TGFb/SMAD pathway often counteracts the pro-inflammatory properties of IFNg, and SMAD4 is a predicted upstream regulator of the DEGs (Fig. 2b). We therefore investigated the effects of survivin inhibition on this pathway (Fig. 4d). Among the top DEGs (nominal $p < 0.005$; Supplementary Fig. 3), we

found upregulation of (1) the E3 ubiquitin ligases *SMURF2, SPSB1, SIAH3, LDLRAD4*, and *PMEPA1*, which facilitate proteolysis required for T-cell reprogramming; (2) *SMAD7* and its co-repressors *SKI* and *SKIL*, which physically interact with the receptor-activated SMADs; and (3) the chromatin-binding SMAD3 co-factors *JUN, FOXO1,* and *BACH1* (Fig. 4e).

In agreement with the increased glycolytic activity of PFKFB3 and LDHA, which control the NOTCH1 and FOXO1 pathways[29-31], survivin inhibition increased mRNA levels of *FOXO1* and *NOTCH1* (Fig. 4e). Consequently, $CD4^+$ cells expressed higher levels of the surface receptors *CD44, IL21R, ITGA5,* and *CXCR3* downstream of NOTCH1 and the FOXO1 target genes *IL2RB, CCR5, CCR7*, and *CXCR4* (Fig. 4b). These transcriptional changes enable the phenotype transition of $CD4^+$ cells.

Survivin colocalizes with IRF1 and SMAD3 on chromatin. To characterize chromatin bound by survivin, we used the JASPAR database of human TF binding sites to analyze motifs in genomic regions covered by the survivin peaks. This analysis revealed enrichment in IRF-binding motifs in all 4 independent ChIP-seq replicates. Predominant among the IRF motifs were IRF1 and IRF8, both containing the conserved GAAA repeat (Fig. 5a). The survivin peaks were also enriched in the composite motifs AP1:IRF (AICE motif, GAAAnnnTGAc/gTCA) and SPI1:IRF (EICE motif, GGAAnnGAAA). Multiple binding sites for each motif were frequently present in a single survivin peak. The ISRE motif (GRAASTGAAAST), which bound two IRFs, was also enriched compared to the whole genome, yet infrequent within the survivin peaks (Fig. 5a).

To connect survivin peaks with transcription, we annotated the whole set of survivin-ChIP peaks to open chromatin in aCD3/aCD28 activated $CD4^+$ cells, using ATAC-seq data (GSE138767[24]). We found that 12.3% (2 h) and 21.5% (4 h of cell stimulation) of the peaks were located within 0–10 kb of open chromatin regions. An independent *de novo* motif search in those survivin peaks revealed up to 4.88-fold enrichment in the binding motifs of IRF1 and the SMAD3/SMAD4 complex, against the randomized background of all open chromatin (Fig. 5B and Supplementary Fig. 4a). No enrichment in JUND and JUN motifs was found. These finding confirmed the functional specificity of survivin binding.

Next, we looked for evidence of physical interaction between survivin and the predicted TF partners, we immunoprecipitated survivin from lysates of THP1 cells. After affinity isolation, protein denaturation, and separation by electrophoresis, western blotting with specific antibodies showed that IRF1 and SMAD3 co-precipitated with survivin (Fig. 5c). Neither IRF8 nor c-MYC, JUN, or JUND were identified in the precipitated material from two independent experiments.

Thus, survivin is recruited to open chromatin containing sequence-specific motifs through its binding to IRF1 and SMAD3. This finding provides molecular evidence that the IRF/survivin/SMAD3 complex helps coordinate the survivin-dependent transcriptional control we observed in the functional experiments (Figs. 3 and 4).

IRF1 and SMAD3 partner with survivin to regulate gene transcription. Since survivin-ChIP peaks accumulated in regulatory chromatin occupied by enhancers (Fig. 2c), we analyzed their presence in the

cis-REs of the top protein-coding DEGs (Supplementary Fig. 3). Using the likelihood score for the enhancer–gene pairing[32], we identified 117 REs that were paired to DEGs and associated with survivin peaks within 0–10 kb and 852 REs with no survivin peaks (Fig. 6a, b). These two groups of REs were similar in GeneHancer (GH) score, length/size of REs, and distance to the transcription start site (TSS) (Supplementary Fig. 5a).

Among the TF ChIP-seq peaks that co-localized with survivin peaks (10% overlap, 0-kb flanks) in ChIP-seq datasets (Fig. 2d), 58 TFs were expressed in $CD4^+$ cells and were more abundant in survivin-containing REs than in the whole genome and or in the remaining REs (all $p<10^{-3}$) (Fig. 6c). IRF1 and SMAD3 were among the most frequent and abundant survivin partners in REs paired to DEGs, as shown by density distribution analysis (Fig. 6d). Principal component analysis of the distribution of the enriched TFs across the REs, followed by unsupervised clustering of the components (Fig. 6e) revealed that REs clustered by total density of TFs (TF-poor and TF-rich) (Supplementary Fig. 5b) rather than by gene association and further by association of TFs with IRF1 or SMAD3 (Fig. 6e). Thus, survivin is present in TF complexes with distinct functions and diverse protein compositions.

Using the BioGrid database to analyze protein–protein interactions, we identified histone acetyltransferase EP300 and glycogen synthetase kinase 3B as the only common interactors of IRF1 and SMAD3 (Fig. 6f). EP300, a polyvalent protein that recruits TFs to distant enhancers, was enriched in survivin-containing REs and physically interacted with several other enriched TFs (Fig. 6e, f), providing a broad platform for building multiprotein complexes. Some of the IRF1 and SMAD3 interactors were differentially expressed in *BIRC5*^{hi}$CD4^+$ cells of RA patients (Fig. 6g, Supplementary Fig. 4b, c).

Survivin has a specific pattern of transcriptional regulation. To explore the mode of survivin-specific transcriptional regulation, we analyzed chromatin regions containing genes highly sensitive to survivin inhibition. Several common features emerged, including (1) long-range interactions between survivin-containing REs and the promoters of target genes, (2) the location of survivin-containing REs among REs clustered into regulatory modules, and (3) the location of survivin-containing REs on repressed/poised chromatin. These features are clearly seen in three genes critical for survivin-dependent metabolism in $CD4^+$ cells: *PFKFB3*, *BIRC2,* and *SMURF2* (Fig. 7a–c).

PFKFB3 was the main target of the survivin-dependent metabolic effects in $CD4^+$ cells. We identified 4 survivin-ChIP peaks associated with 5 high-scored REs paired to *PFKFB3* (Fig. 7a). These REs covered a region extending from ~20 kb upstream to 100 kb downstream of *PFKFB3*. Both the upstream and the downstream REs contained ChIP peaks for IRF1 and SMAD3 grouped together with the survivin peaks (Fig. 6e). Publicly available data (*e.g.*,, HiC, eQTL) indicated internal connection between these REs and the *PFKFB3* promoter. Functional segmentation in $CD4^+$ cells annotate the upstream REs to the active promoter and the downstream REs to the repressed region. Thus, activation of those areas after survivin inhibition would enhance *PFKFB3* expression. Near the upstream REs were single nucleotide polymorphisms (SNPs) identified by genome-wide association studies (GWAS) provide additional weight to those loci and implicated in T-cell-mediated disorders, including latent autoimmune diabetes,

and thyroiditis at the upstream REs and type 1 diabetes, RA, thyroiditis, and celiac disease at the downstream REs (Fig. 7a). Thus, the binding of survivin to those REs may be important for *PFKFB3* expression and glucose utilization in T cells.

BIRC2 was significantly upregulated by survivin inhibition. Fig. 7b shows an extended region of ~550 kb containing 26 REs paired to and surrounding *BIRC2*. Two of these REs, located ~100 kb and ~400 kb downstream of the TSS, were associated with 3 survivin-ChIP peaks. Despite their distant location, both REs were strongly linked to *BIRC2* (GH scores of 1.56 and 10.95, respectively). Both REs contained multiple IRF1 and SMAD3 ChIP-seq peaks and were located within the repressed/poised chromatin according to the functional chromatin segmentation in $CD4^+$ cells. The *BIRC2* locus contains few immunologically relevant SNPs.

Survivin activated transcription of *SMURF2*. Regulatory chromatin around *SMURF2* forms a dense cluster of 25 adjacent REs that span the region of ~100 kb upstream of the TSS and cover the gene start (Fig. 7c). Four survivin peaks are annotated to 12 of those REs, 11 of which were in poised/inactive chromatin. An additional survivin peak was in *SMURF2*, outside of any RE. REs paired to *SMURF2* differed in length, TF density, and presence of survivin partners IRF1 and SMAD3 (Fig. 6e). Simultaneous activation of the poised REs triggered by survivin inhibition was predicted by te RoadMap data that reveal a higher-order regulatory unit at this site. Therefore, cooperative activation of the clustered REs is a plausible mechanism for the pronounced upregulation of *SMURF2* expression.

Discussion

This study demonstrates a survivin-dependent mechanism of metabolic adaptation existing in the IFNγ-producing $CD4^+$ cells. We show that nuclear survivin has a genome-wide and motif specific binding to chromatin with unappreciated function in gene transcription control. The exact position of survivin binding is defined here by its physical interaction with the TFs IRF1 and SMAD3. We describe that the IRF1/survivin/SMAD3 complex keeps control of *PFKFB3*, the major point of metabolic adaptation for autoreactive T cells, and other genes responsible for glycolysis and sugar transport through binding to clusters of REs at a distance from the target genes. Thus, survivin binding to chromatin acts as epigenetic check-point coordinating metabolic switch required for effector function of the IFNγ-producing $CD4^+$ cells.

We found that survivin/*BIRC5*^{hi} $CD4^+$ cells have elevated expression of *HIF1A* and the canonical HIF-1a targets, including numerous glycolytic enzymes and hypoxia-sensing proteins, consistent with reports indicating HIF1α-dependent expression pattern of survivin[33–35]. In RA, hypoxia is an important mechanism of immune cell invasion and excessive proliferation in joints[36,37]. We also found that survivin is an essential mediator of the metabolic effects of HIF1α and links them to IFNg-driven inflammation. By analyzing DEGs, we found effects of survivin downstream of HIF1a. Inhibition of survivin repressed the hypoxia-sensing proteins *SESN2, PYHIN2*, and *NLRX1*, which inhibited GLUT1 expression and glucose

uptake. Subsequently, this strengthened c-Myc driven glutamate metabolism seen in upregulation of the major glutamine transporter *SLC1A4* and neutral amino acid transporter *SLC7A5*[38].

Repression of the key glycolytic enzyme PFKFB3 was central for the survivin-dependent metabolic effects in $CD4^+$ cells and led to activation of LDHA and aerobic glycolysis and a cessation of the pentose phosphate pathway. *PFKFB3* is highly responsive to a growth factors, inflammation, and ischemia, all of which activate estrogen receptor-, hypoxia-, or progesterone response elements on its promoter[39]. Thus, maintenance of *PFKFB3* repression requires energy. Integrative analysis of ChIP-seq and protein binding data identified IRF1/survivin/Smad3 complexes as potent repressors of the REs paired to *PFKFB3*. Inhibition of survivin activated *PFKFB3* expression and restored conventional aerobic glycolysis through the TCA cycle. This survivin-dependent change in the mode of glucose utilisation is consistent with the logical connection between hypoxia, survivin, and IRF1-dependent effector function of $CD4^+$ cells. IRF1 is the lineage-specific TF that mediates IFNg signaling and forms the phenotype of Th1 cells. Survivin is mobilized to chromatin sequences containing IRF-binding motifs and directly binds IRF1, enabling it to help regulate the transcriptional of IRF1 target genes. Inhibition of survivin significantly impaired both IFNg production and the sensitivity of $CD4^+$ cells to IFNg stimulation, which is required to maintain their effector phenotype and chronic inflammation.

Our findings showed that survivin represses TGFb/SMAD-dependent processes in $CD4^+$ cells. Indeed, genes encoding proteins downstream of TGFb/SMAD were among the top DEGs upregulated after survivin inhibition, and SMAD3 was one of the most densely present TFs in the REs of those DEGs. Finally, our findings showed a close interaction between survivin and SMAD3, as shown by immunoprecipitation studies. JUN did not interact with survivin in western blot and was not enriched in the survivin peaks in open chromatin; but neither of those findings exclude the possibility of an interaction between AP-1 TFs and SMAD3[40] or their consolidating effect on the IRF1/survivin/SMAD3 complex. Conversely, SMAD3/4 and AP1 proteins are frequently found on distant *cis*-regulatory regions, where they facilitate promoter–enhancer interactions through chromatin looping and triggering transcription[41]. Cell activation with TGFb elicits a widespread SMAD-dependent increase in chromatin accessibility[62]. Hypoxia affects the level of SMAD3 phosphorylation and SMAD4 binding[42,43]. Hypothetically, formation of the survivin/SMAD3 complex might anchor SMAD3 to inactive/poised chromatin, protecting it from degradation and creating a predisposition for rapid changes in transcriptional activity, as observed in our study.

The identified interaction within the IRF1/survivin/SMAD3 complex could participate in transcriptional regulation by other mechanisms. The EP300/CREB1 complex is involved in RNA polymerase II–dependent recruitment of TFs to distant REs in inactive/poised chromatin, where REs paired to DEGs are predominantly located. Both EP300 and CREB1 ChIP-seq binding sites were significantly enriched in REs and were the only common interactors for IRF1 and SMAD3. An interaction between EP300 and SMAD3 could facilitate the upregulation of the DEGs we detects after survivin inhibition. In this scenario, survivin functions as a guardian of the functional chromatin state by preventing this interaction. Remarkably, the

activity of EP300/CREB1 is mediated by glucose[44] and integrates the immune processes initiated by IFNγ[45] and TGFb-signaling, potentially by patronising the epigenetic activity of the IRF1/survivin/SMAD3 complex.

In agreement with our findings, repression of *PFKFB3*, which switched glucose processing to the pentose phosphate pathway, has been suggested as the major point of metabolic adaptation for autoreactive T cells in RA [6]. In type 1 diabetes, multiple sclerosis, and systemic lupus erythematosus, the cells experience no energetic starvation and rely on pyruvate kinase–dependent hyperproduction of lactate[46–48]. Experimentally, inhibition of PFKFB3 could restore the metabolic alterations and disable the effector function of T cells in multiple sclerosis, graft-versus-host disease, and type 1 diabetes[46,49]. It could also induce insulin resistance and accelerate inflammation in these conditions[50,51]. GWAS have shown that the genomic region around *PFKFB3* harbors several critical polymorphisms associated with autoimmune diabetes, RA, and celiac disease, suggesting that this region is strongly linked to metabolic and autoimmune conditions through variation in T-cell transcription[52–54]. Recently, new SNPs near *PFKFB3* have been linked to differences in TNFa and IL6 production[55].

Our studies identify a novel epigenetic mechanism that connects regulation of the *PFKFB3* locus to the metabolic phenotype of effector $CD4^+$ cells. Although we studied primary $CD4^+$ cells from RA patients and healthy women, our findings deepen our understanding of the molecular mechanisms of autoimmunity. The tight interaction within the IRF1/survivin/SMAD3 complex maintains expression of IFN-sensitive genes that are clinically relevant to several autoimmune diseases, including RA[26], systemic lupus erythematosus[27], and Sjögren's syndrome[28]. The fundamental role of survivin in bridging the transcriptional programs governed by IRF1 and SMAD3 sheds light on the regulation of the balance between IFNγ- and TGFb-dependent processes. Pharmacological interventions that selectively target these molecular interactions of survivin could be an attractive approach to improve control of IFNγ-dependent autoimmunity.

Materials And Methods

Patients. Blood samples of 46 RA patients and 7 healthy female controls were collected at the Rheumatology Clinic, Sahlgrenska Hospital, Gothenburg. Clinical characteristics of the patients are shown in Supplementary Table 2. All RA patients fulfilled the EULAR/ACR classification criteria[56] and gave written informed consent before the blood sampling. The study was approved by the Swedish Ethical Evaluation Board (659-2011) and done in accordance with the Declaration of Helsinki. The trial is registered at ClinicalTrials.gov (ID NCT03449589).

Isolation and stimulation of $CD4^+$ cells. Human peripheral blood mononuclear cells (PBMC) were isolated from venous peripheral blood by density gradient separation on Lymphoprep (Axis-Shield PoC As, Dundee, Scotland). $CD4^+$ cells were isolated by positive selection (Invitrogen, 11331D), and cultured ($1.25x10^6$ cells/ml) in complete RPMI-medium supplemented with concanavalin A (ConA, 0.625 µg/ml,

Sigma-Aldrich), and lipopolysaccharide (LPS) (5 µg/ml, Sigma-Aldrich), for 24 or 72 h. In the inhibition experiments, $CD4^+$ cells were cultured in wells coated with anti-CD3 antibody (0.5 mg/ml; OKT3, Sigma-Aldrich), in RPMI-medium supplemented with the survivin inhibitor YM155[25] (0 or 10 nM; Selleck Chemicals, Houston, TX) for 24 or 72 h. The cells were stimulated with recombinant IFNg (50 ng/ml; Peprotech, Cranbury, NJ, USA) during the last 2 h.

Flow cytometry analysis. Freshly isolated PBMC were stimulated overnight with ConA (0.625 µg/ml), harvested, and stained for flow cytometry as described[9] using antibodies to the following human surface antigens: CD4-APCH7 (SK3), CD8-PerCP (SK1), , CD62L-PECy7 (DREG-56), CD27-APC (L128), and CD19-V500 (all from BD Biosciences, Franklin Lakes, NJ, USA) and (H1B19) and CD45RA-BV421 (HI100) (both from BioLegend). Cells were then fixed and permeabilized with a Cytofix-Cytoperm fixation/permeabilization kit (BD) and stained with anti-survivin (91630, R&D Systems, Minneapolis, MN, USA) and isotype control (mouse IgG1κ, R&D Systems). The cells were sorted with a FACSCantoII flow cytometer (BD), and the data were analyzed with FlowJo software (BD, v.10.7) and fluorescence minus one controls.

Chromatin immunoprecipitation, library preparation, and sequencing. $CD4^+$ cells isolated from 12 women were stimulated with ConA+LPS for 72 h and pooled in 4 independent samples for chromatin purification. The cells were cross-linked and lysed with the EpiTect ChIP OneDay kit (Qiagen), as recommended by the manufacturer. After sonication to shear the chromatin, cellular debris was removed by pelleting. After pre-clearing, 1% of the sample was saved as an input fraction and used as background for nonspecific chromatin binding. Pre-cleared chromatin was incubated with 2 µg of anti-survivin (10811, Santa Cruz Biotechnology, Santa Cruz, CA, USA). The immune complexes were washed, the cross-links were reversed, and the DNA was purified with the EpiTect ChIP OneDay kit (Qiagen) as recommended by the manufacturer. The quality of purified DNA was assessed with TapeStation (Agilent, Santa Clara, CA, USA). DNA libraries were prepared with ThruPLEX (Rubicon) and sequenced with a Hiseq2000 sequencing system (Illumina) according to the manufacturer's protocols. Bcl-files were converted and demultiplexed to fastq with bcl2fastq (Illumina).

Transcriptional sequencing (RNA-seq). RNA from $CD4^+$ cell cultures was prepared with the Norgen Total Micro mRNA kit (Norgen, Ontario, Canada). Quality control was done with a Bioanalyzer RNA6000 Pico on an Agilent2100 (Agilent, St.Clara, CA, USA). Deep sequencing was done by RNA-seq (Hiseq2000, Illumina) at the LifeScience Laboratory, Huddinge, Sweden. Raw sequence data were obtained in Bcl files and converted to fastq text format with bcl2fastq. RNA-seq results were validated by qRT-PCR as described below.

RNA-seq analysis. Transcripts were mapped with the UCSC Genome Browser using the annotation set for the hg38 human genome assembly and analyzed with the core Bioconductor packages in R-studio (v.3.6.3). DEGs were identified with DESeq2 (v.1.26.0) with Benjamini-Hochberg adjustment for multiple testing. Volcano plots were prepared with EnhancedVolcano (v.1.4.0). Correlation analysis was done with Hmisc (v.4.5), and the correlation heatmap was built with Corrplot (v.0.85). RNA-seq data were clustered

with the Spearman correlation for distance (factoextra, v.1.0.7). WardD2 was used for hierarchical clustering.

Conventional qPCR. RNA was isolated with the Total RNA Purification Kit (17200, Norgen Biotek). RNA concentration and quality were evaluated with a NanoDrop spectrophotometer (Thermo Fisher Scientific) and Experion electrophoresis system (Bio-Rad Laboratories). cDNA was synthesized from RNA (400 ng) with the High-Capacity cDNA Reverse Transcription Kit (Applied Biosystems, Foster City, CA, USA). Real-time amplification was done with RT2 SYBR Green qPCR Mastermix (Qiagen) and a ViiA 7 Real-Time PCR System (Thermo Fisher Scientific) as described[10]. Primers used are shown in Supplementary Table 3. Expression was calculated by the ddCt method.

Affinity immunoprecipitation and western blotting. Human monocyte leukemia cell line THP-1 was cultured at a density of 3-10×10^5 cells/ml in RPMI1640 medium supplemented with 10% fetal bovine serum at 37°C in a humidified 5% CO_2 atmosphere. Cells were lysed in IP Lysis Buffer (87787, Pierce) supplemented with protease inhibitors (Complete Mini, Roche), and immunoprecipitation (IP) was done with antibodies against survivin (RnD AF886) coupled to Dynabeads protein G beads (Dynabeads Protein G Immunoprecipitation Kit, 10007D, ThermoFisher Scientific), and cross-linked with bis(sulfosuccinimidyl)suberate (A39266, Pierce).

For western blotting, 30 mg of total protein from whole-cell lysates and the IP material was separated on NuPage 4–12% Bis–Tris gels (Novex). Proteins were transferred to polyvinylidene difluoride membranes (iBlot, Invitrogen), blocked with a solution of Tris-buffered saline containing Tween-20 and 3% bovine serum albumin, and incubated first with antibodies against IRF1 (H-8, sc-74530), IRF8 (E-9, sc-365042), JUND (D-9, sc-271938), SMAD3 (38-Q, sc-101154), MAX (H-2, sc-8011), and MYC (9E10, sc-40) (all from Santa Cruz Biotechnology; 1:500) and then with peroxidase-conjugated anti-mouse antibodies (NA931, GE Healthcare, Chicago, IL; 1:4000). Bands were visualized with ECL Select Western Blotting Detection Reagent (Amersham) and a ChemiDoc imager and Quantity One software (Bio-Rad Laboratories).

Cytokine measurement. Cytokine levels in supernatants of $CD4^+$ cells were measured with a sandwich enzyme-linked immune assay. Briefly, high-performance 384-well plates (Corning Plasticware, Corning, NY, USA) were coated with capture antibody, blocked, and developed according to the manufacturers' instructions. IFNg (PelikineM1933, detection limit 3 pg/ml, Sanquin, Amsterdam, The Netherlands), IL10 (DY217B, detection limit 15 pg/ml), IL9 (DY209, detection limit 1 pg/ml), IL13 (DY213, detection limit 50 pg/ml), and IL4 (DY204, detection limit 0.25 pg/ml (all from R&D Systems). Developed plates were read in a SpectraMax340 Microplate reader (Molecular Devices, San Jose, CA, USA), and absolute protein levels were calculated after serial dilutions of the recombinant protein provided by the manufacturer.

Glucose uptake assay. Glucose uptake was monitored with 2NBDG (Abcam). $CD4^+$ cells were cultured for 24 h in anti-CD3 coated plates (0.5 mg/ml) supplemented with IFNg (50 ng/ml) and YM155 (0 and 10 nM). Cells were starved in glucose-free RPMI-medium for 2 h and then supplemented with 2-NBDG (100

μM). 2NBDG uptake was registered after 30 min using flow cytometry (Verse, BD) and quantified as the ratio of mean fluorescence intensity to baseline.

ChIP-seq analysis. The fastq sequencing files were mapped to the human reference genome (hg38) with the STAR aligner[57]; the alignIntronMax flag was set to 1 for end-to-end mapping. The quality of sequenced material was assessed with the FastQC tool and MultiQC (v.0.9dev0) (Babraham Institute, Cambridge, UK). Peaks were called with MACS2 algorythm for narrow peaks and default parameters. Peaks were filtered for the survivin antibody IP fraction (IP) and unprocessed DNA (Input) and annotated with HOMER software[58] in standard mode to the closest TSS with no distance restriction. A set of peaks with enrichment versus surrounding region and Input (adjusted $p < 10^{-5}$) was identified and quantified separately for each sample. Peaks that overlapped by at least 1 nucleotide in several samples were merged as survivin-ChIP peaks. Peaks in all samples were scored by the number of tags of difference between IP and Input (average of these differences between samples). HOMER (findMotifsGenome.pl) and the homer2 engine were used for *de novo* motif discovery and motif scanning. The most common *de novo* motifs were identified separately for each IP sample and examined for detected motifs in the JASPAR database of human TF binding sites[59]. The Input bed regions were compared with random global controls generated by the service to match the input dataset. For analysis we selected the following binding motifs: JUN.MA0488.1, JUND_2.MA0492.1, IRF1.MA0050.2 and the combined SMAD2_SMAD3_SMAD4.MA0513.1. For each motif, we estimated global control-based *p* value and fold enrichment. For association with open chromatin, survivin-ChIP peaks within 10 kb from ATAC-seq peaks were detected in $CD4^+$ T cells after 2 or 4 h of stimulation[24].

Genome distribution of survivin-ChIP peaks. Genome UCSC annotation hg38 (http://genome.ucsc.edu/; accessed April 10, 2021) was used to compare the whole-interval set of survivin-ChIP peaks with the set of functional genomic regions. TSSs were defined based on chromStart or chromEnd positions in GENCODE v36. Promoters were defined as regions 5 kb upstream plus 1 kb upstream of the TSS annotated as above. The CTCF-binding sites were accessed according to ENSEMBL regulatory build (v103, 2020 (http://www.ensembl.org/info/docs/funcgen/regulatory_build.html; accessed March 1, 2021) (177,376 elements). Insulator sites for all aggregated cells were defined according to ENCODE v5, 2020) (https://screen.encodeproject.org/, https://api.wenglab.org/screen_v13/fdownloads/GRCh38-ccREs.CTCF-only.bed file; accessed March 1, 2021) (56,766 elements). Enhancers were selected with the integrated GeneHancer database (v4.4, https://www.genecards.org/GeneHancer_version_4-4; accessed January 5, 2021. GH score >0.7).

For genomic interval datasets, including survivin-ChIP peaks and REs, the Table Browser for the hg38 human genome assembly (http://genome.ucsc.edu/cgi-bin/hgTables) and Galaxy suite tools (https://usegalaxy.org/) were used for estimating distances between nearest intervals, merging, overlapping, calculating genomic coverage, and other standard procedures. The genome-wide distribution of survivin-ChIP peaks was initially screened with the *cis*-regulatory annotation system (CEAS v0.9.8; accessed November 1, 2020 with Cistrome Galaxy, http://cistrome.org/ap/root). For enrichment analysis,

we used the list of all survivin-ChIP peaks and the fraction of them located within 100 kb of the known genes. To estimate pairwise distances and statistical significance of pairwise interval overlaps for survivin-ChIP peaks with genome elements defined above, we used Bedtools suite (https://github.com/arq5x/bedtools2; accessed 01feb2021–15apr 2021). For each comparison, a pairwise, two-tailed Fisher's exact test was used. Comparison was based on initial survivin-ChIP peak positions as intervals and extended regions with 1-kb, 10-kb and 50-kb flanks.

Peak colocalization analysis with transcription regulators. To identify transcription regulators near survivin-ChIP peaks, we used the ReMap database (http://remap.univ-amu.fr/; accessed November 15, 2020) for colocalization analysis of aggregated cell- and tissue-agnostic human ChIP-seq datasets of 1034 transcriptional regulator. ReMapEnrich R-script (https://github.com/remap-cisreg/ReMapEnrich; accessed November 15, 2020) was used for colocalization enrichment analysis. The hg38 human genome assembly was used for all comparisons. Two-tailed *p* values were estimated and normalized with the Benjamini-Yekutielli test, using the maximal allowed value of shuffled genomic regions for each dataset ($n = 15$), kept on the same chromosome (shuffling genomic regions parameter byChrom=TRUE). The default fraction of minimal overlap for input and catalogue intervals was set to 10%. Bed interval files of survivin-ChIP peaks with 0- and 100-kb flanks were prepared. The dataset with 0-kb flanks was compared with the Universe sets of genomic regions, defined as within 1 Mb of the same ChIP-seq peaks. For analysis of the regulatory chromatin paired with DEGs, input bedfiles were selected according to their distance from the genome region containing REs paired to DEGs; bedfiles for individual TFs were downloaded from ReMap2020.

Analysis of candidate partner TFs. TFs with statistically significant enrichment of overlaps (q value <0.05, $n > 100$) were selected. TFs that were enriched with respect to the genomic background were identified within each RE by using ReMap database, as described above. A subset of TFs enriched within the survivin-associated REs was identified by chi-square test (chisq.test, R-studio) and false-discovery rate correction (R-studio). To explore the involvement of these TFs in regulating DEGs, we prepared the presence matrix (1/0 type), excluded regions with 0 overlaps with top TFs, and did a principal component analysis with singular value decomposition imputation. Hierarchical clustering of TFs was done with Canberra or Euclidean distances (prcomp, hclust, R-studio). False discovery rate–adjusted *p* values and the ratio between the survivin-associated and survivin-independent REs per 1 Mb was estimated.

Gene set enrichment analysis. DEGs were compared to all protein-coding human genes (by default) by gene set enrichment analysis (https://www.gsea-msigdb.org/gsea/index.jsp; accessed November 15, 2020). TFs with significant overlap between ChIP-seq and survivin-ChIP peaks were analyzed in comparison to all 1034 transcriptional regulators in ReMap2020 (accessed November 20, 2020). General functional categories for DEGs and TFs were annotated with MetaScape (https://metascape.org/gp/index.html; accessed November 15, 2020). Gene Ontology terms and the TRRUST database were used for pathway analysis. Pathways were selected by minimal gene overlap equal to 2, $p < 0.05$, and a minimal enrichment threshold of 1.3. Terms retrieved from Gene Ontology

biological processes were grouped by medium term similarity of 0.7 and arranged on the semantic similarity scale coordinates with ReViGo (http://revigo.irb.hr/; accessed December 1,2020).

Genome-wide association data. Known genetic associations of the analyzed regulatory regions of DEGs were examined with NHGRI's collection of GWAS (http://genome.ucsc.edu/; accessed May 1, 2021). All published GWAS SNPs were included without *p* value or ancestry filtering. A subset of relevant SNPs was selected by keyword searches for traits of individual autoimmune disorders in Table Browser[60].

Chromatin functional segmentation data in $CD4^+$ cells. Primary functional chromatin segmentation was accessed by using NIH Roadmap Epigenomic Project data for activated $CD4^+$ T cells (E042: $CD4^+$_$CD25^-$_$IL17^+$_PMA/Ionomyc_stimulated_Th17_Primary_Cells; accessed with the Washington University Epigenomic Browser http://epigenomegateway.wustl.edu/browser/roadmap/ on May 1, 2021). The default color scheme was applied to chromatin segments of active enhancers, transcribed regions, and repressed and poised loci.

Data availability. RNA sequencing data and survivin ChIP-Seq data (raw data and processed files) of $CD4^+$ T cells that support the findings of this study have been depositied in NCBI GEO. All other relevant data supporting the key findings of this study are available within the article and its Supplementary Information files from the corresponding author upon reasonable request. Source data are provided in this paper.

References

1. Shyer, J. A., Flavell, R. A. & Bailis, W. Metabolic signaling in t cells. *Cell Res* **30**, 649–659 (2020).
2. Wang, R. *et al.* The transcription factor myc controls metabolic reprogramming upon t lymphocyte activation. *Immunity* **35**, 871–882 (2011).
3. Phan, A. T., Goldrath, A. W. & Glass, C. K. Metabolic and epigenetic coordination of t cell and macrophage immunity. *Immunity* **46**, 714–729 (2017).
4. Jacobs, S. R. *et al.* Glucose uptake is limiting in t cell activation and requires cd28-mediated akt-dependent and independent pathways. *J Immunol* **180**, 4476–4486 (2008).
5. Gubser, P. M. *et al.* Rapid effector function of memory cd8+ t cells requires an immediate-early glycolytic switch. *Nat Immunol* **14**, 1064–1072 (2013).
6. Jiang, J., Zhao, M., Chang, C., Wu, H. & Lu, Q. Type i interferons in the pathogenesis and treatment of autoimmune diseases. *Clin Rev Allergy Immunol* **59**, 248–272 (2020).
7. Fukuda, S. *et al.* Survivin modulates genes with divergent molecular functions and regulates proliferation of hematopoietic stem cells through evi-1. *Leukemia* **29**, 433–440 (2015).
8. Paydas, S., Ergin, M., Seydaoglu, G., Erdogan, S. & Yavuz, S. Prognostic [corrected] significance of angiogenic/lymphangiogenic, anti-apoptotic, inflammatory and viral factors in 88 cases with diffuse large b cell lymphoma and review of the literature. *Leuk Res* **33**, 1627–1635 (2009).

9. Andersson, K. M. *et al.* Survivin co-ordinates formation of follicular t-cells acting in synergy with bcl-6. *Oncotarget* **6**, 20043–20057 (2015).
10. Andersson, K. M. *et al.* Survivin controls biogenesis of microrna in smokers: A link to pathogenesis of rheumatoid arthritis. *Biochim Biophys Acta Mol Basis Dis* **1863**, 663–673 (2017).
11. Kostrouchova, M., Kostrouch, Z., Saudek, V., Piatigorsky, J. & Rall, J. E. Bir-1, a caenorhabditis elegans homologue of survivin, regulates transcription and development. *Proc Natl Acad Sci U S A* **100**, 5240–5245 (2003).
12. Okada, H. *et al.* Survivin loss in thymocytes triggers p53-mediated growth arrest and p53-independent cell death. *J Exp Med* **199**, 399–410 (2004).
13. Xing, Z., Conway, E. M., Kang, C. & Winoto, A. Essential role of survivin, an inhibitor of apoptosis protein, in t cell development, maturation, and homeostasis. *J Exp Med* **199**, 69–80 (2004).
14. Song, J., So, T. & Croft, M. Activation of nf-kappab1 by ox40 contributes to antigen-driven t cell expansion and survival. *J Immunol* **180**, 7240–7248 (2008).
15. Gravina, G. *et al.* Survivin in autoimmune diseases. *Autoimmun Rev* **16**, 845–855 (2017).
16. Rahban, D. *et al.* Genetic polymorphisms and epigenetic regulation of survivin encoding gene, birc5, in multiple sclerosis patients. *BMC Immunol* **20**, 30 (2019).
17. Zhang, X., Ciesielski, M., Fenstermaker, R. A., Kaminski, H. J. & Kusner, L. L. The presence of survivin on b cells from myasthenia gravis patients and the potential of an antibody to a modified survivin peptide to alleviate weakness in an animal model. *J Immunol* **205**, 1743–1751 (2020).
18. Locke, F. L. *et al.* Survivin-specific cd4+ t cells are decreased in patients with survivin-positive myeloma. *J Immunother Cancer* **3**, 20 (2015).
19. Andersson, K. M., Svensson, M. N., Erlandsson, M. C., Jonsson, I. M. & Bokarewa, M. I. Down-regulation of survivin alleviates experimental arthritis. *J Leukoc Biol* **97**, 135–145 (2015).
20. Levitsky, A., Erlandsson, M. C., van Vollenhoven, R. F. & Bokarewa, M. I. Serum survivin predicts responses to treatment in active rheumatoid arthritis: A post hoc analysis from the swefot trial. *BMC Med* **13**, 247 (2015).
21. Svensson, B., Hafstrom, I., Erlandsson, M. C., Forslind, K. & Bokarewa, M. I. Smoking in combination with antibodies to cyclic citrullinated peptides is associated with persistently high levels of survivin in early rheumatoid arthritis: A prospective cohort study. *Arthritis Res Ther* **16**, R12 (2014).
22. Mahnke, Y. D., Brodie, T. M., Sallusto, F., Roederer, M. & Lugli, E. The who's who of t-cell differentiation: Human memory t-cell subsets. *Eur J Immunol* **43**, 2797–2809 (2013).
23. Winter, S. C. *et al.* Relation of a hypoxia metagene derived from head and neck cancer to prognosis of multiple cancers. *Cancer Res* **67**, 3441–3449 (2007).
24. Yang, J. *et al.* Analysis of chromatin organization and gene expression in t cells identifies functional genes for rheumatoid arthritis. *Nat Commun* **11**, 4402 (2020).
25. Nakahara, T. *et al.* Ym155, a novel small-molecule survivin suppressant, induces regression of established human hormone-refractory prostate tumor xenografts. *Cancer Res* **67**, 8014–8021

(2007).

26. Lubbers, J. *et al.* The type i ifn signature as a biomarker of preclinical rheumatoid arthritis. *Ann Rheum Dis* **72**, 776–780 (2013).
27. Bennett, L. *et al.* Interferon and granulopoiesis signatures in systemic lupus erythematosus blood. *J Exp Med* **197**, 711–723 (2003).
28. Hjelmervik, T. O., Petersen, K., Jonassen, I., Jonsson, R. & Bolstad, A. I. Gene expression profiling of minor salivary glands clearly distinguishes primary sjogren's syndrome patients from healthy control subjects. *Arthritis Rheum* **52**, 1534–1544 (2005).
29. De Bock, K. *et al.* Role of pfkfb3-driven glycolysis in vessel sprouting. *Cell* **154**, 651–663 (2013).
30. Maekawa, Y. *et al.* Notch controls the survival of memory cd4+ t cells by regulating glucose uptake. *Nat Med* **21**, 55–61 (2015).
31. Xu, K. *et al.* Glycolysis fuels phosphoinositide 3-kinase signaling to bolster t cell immunity. *Science* **371**, 405–410 (2021).
32. Fishilevich, S. *et al.* Genehancer: Genome-wide integration of enhancers and target genes in genecards. *Database (Oxford)* **2017** (2017).
33. Chen, Y. Q., Zhao, C. L. & Li, W. Effect of hypoxia-inducible factor-1alpha on transcription of survivin in non-small cell lung cancer. *J Exp Clin Cancer Res* **28**, 29 (2009).
34. Pawlus, M. R., Wang, L. & Hu, C. J. Stat3 and hif1alpha cooperatively activate hif1 target genes in mda-mb-231 and rcc4 cells. *Oncogene* **33**, 1670–1679 (2014).
35. Peng, X. H. *et al.* Cross-talk between epidermal growth factor receptor and hypoxia-inducible factor-1alpha signal pathways increases resistance to apoptosis by up-regulating survivin gene expression. *J Biol Chem* **281**, 25903–25914 (2006).
36. Taylor, P. C. & Sivakumar, B. Hypoxia and angiogenesis in rheumatoid arthritis. *Curr Opin Rheumatol* **17**, 293–298 (2005).
37. Fearon, U., Canavan, M., Biniecka, M. & Veale, D. J. Hypoxia, mitochondrial dysfunction and synovial invasiveness in rheumatoid arthritis. *Nat Rev Rheumatol* **12**, 385–397 (2016).
38. Bernard, K. *et al.* Glutaminolysis is required for transforming growth factor-beta1-induced myofibroblast differentiation and activation. *J Biol Chem* **293**, 1218–1228 (2018).
39. Shi, L., Pan, H., Liu, Z., Xie, J. & Han, W. Roles of pfkfb3 in cancer. *Signal Transduct Target Ther* **2**, 17044 (2017).
40. Liberati, N. T. *et al.* Smads bind directly to the jun family of ap-1 transcription factors. *Proc Natl Acad Sci U S A* **96**, 4844–4849 (1999).
41. Li, M. *et al.* Core transcription regulatory circuitry orchestrates corneal epithelial homeostasis. *Nat Commun* **12**, 420 (2021).
42. Lin, X. *et al.* Ppm1a functions as a smad phosphatase to terminate tgfbeta signaling. *Cell* **125**, 915–928 (2006).

43. Xu, Q. *et al.* Phosphatase pp2a is essential for th17 differentiation. *Proc Natl Acad Sci U S A* **116**, 982–987 (2019).
44. Gutierrez-Salmeron, M. *et al.* Paradoxical activation of ampk by glucose drives selective ep300 activity in colorectal cancer. *PLoS Biol* **18**, e3000732 (2020).
45. Bouhet, S., Lafont, V., Billard, E., Gross, A. & Dornand, J. The ifngamma-induced stat1-cbp/p300 association, required for a normal response to the cytokine, is disrupted in brucella-infected macrophages. *Microb Pathog* **46**, 88–97 (2009).
46. Martins, C. P. *et al.* Glycolysis inhibition induces functional and metabolic exhaustion of cd4(+) t cells in type 1 diabetes. *Front Immunol* **12**, 669456 (2021).
47. Mathur, D., Lopez-Rodas, G., Casanova, B. & Marti, M. B. Perturbed glucose metabolism: Insights into multiple sclerosis pathogenesis. *Front Neurol* **5**, 250 (2014).
48. Yin, Y. *et al.* Normalization of cd4+ t cell metabolism reverses lupus. *Sci Transl Med* **7**, 274ra218 (2015).
49. Nguyen, H. D. *et al.* Metabolic reprogramming of alloantigen-activated t cells after hematopoietic cell transplantation. *J Clin Invest* **126**, 1337–1352 (2016).
50. Huo, Y. *et al.* Disruption of inducible 6-phosphofructo-2-kinase ameliorates diet-induced adiposity but exacerbates systemic insulin resistance and adipose tissue inflammatory response. *J Biol Chem* **285**, 3713–3721 (2010).
51. Montemurro, C. *et al.* Iapp toxicity activates hif1alpha/pfkfb3 signaling delaying beta-cell loss at the expense of beta-cell function. *Nat Commun* **10**, 2679 (2019).
52. Coenen, M. J. *et al.* Common and different genetic background for rheumatoid arthritis and coeliac disease. *Hum Mol Genet* **18**, 4195–4203 (2009).
53. Cousminer, D. L. *et al.* First genome-wide association study of latent autoimmune diabetes in adults reveals novel insights linking immune and metabolic diabetes. *Diabetes Care* **41**, 2396–2403 (2018).
54. Okada, Y. *et al.* Genetics of rheumatoid arthritis contributes to biology and drug discovery. *Nature* **506**, 376–381 (2014).
55. Keating, S. T. *et al.* Rewiring of glucose metabolism defines trained immunity induced by oxidized low-density lipoprotein. *J Mol Med (Berl)* **98**, 819–831 (2020).
56. Aletaha, D. *et al.* 2010 rheumatoid arthritis classification criteria: An american college of rheumatology/european league against rheumatism collaborative initiative. *Arthritis Rheum* **62**, 2569–2581 (2010).
57. Dobin, A. *et al.* Star: Ultrafast universal rna-seq aligner. *Bioinformatics* **29**, 15–21 (2013).
58. Heinz, S. *et al.* Simple combinations of lineage-determining transcription factors prime cis-regulatory elements required for macrophage and b cell identities. *Mol Cell* **38**, 576–589 (2010).
59. Khan, A. *et al.* Jaspar 2018: Update of the open-access database of transcription factor binding profiles and its web framework. *Nucleic Acids Res* **46**, D260-D266 (2018).

60. Supek, F., Bosnjak, M., Skunca, N. & Smuc, T. Revigo summarizes and visualizes long lists of gene ontology terms. *PLoS One* **6**, e21800 (2011).

Declarations

Author contributions

Conceiving the study, M.B., K.A., GK; collecting materia, M.E., K.A., S.T.S., Z.E., M.B.; Laboratory work, K.A., M.E., M.J.G.B.; Statistical analysis, M.E., K.A., V.C., N.O., M.B., A.D.; drafting the manuscript, M.B., N.O., M.P., G.K., M.E.. All authors discussed and helped interpret the data and provided feedback during preparation of the manuscript.

Acknowledgements

This work was funded by grants from the Swedish Research Council (MB, 521-2017-03025), the Röntgen-Ångström Cluster Framework of the Swedish Research Council (GK, 2015-06099), the Swedish Association against Rheumatism (MB, R-566961), the King Gustaf V:s 80-year Foundation (MB), the Regional agreement on medical training and clinical research between the Western Götaland county council and the University of Gothenburg (MB, ALFGBG-717681), the University of Gothenburg, and Southern Älvsborg Hospital, Borås, Sweden (ZE).

Additional Information

Competing interests: The authors declare no competing interests.

Figures

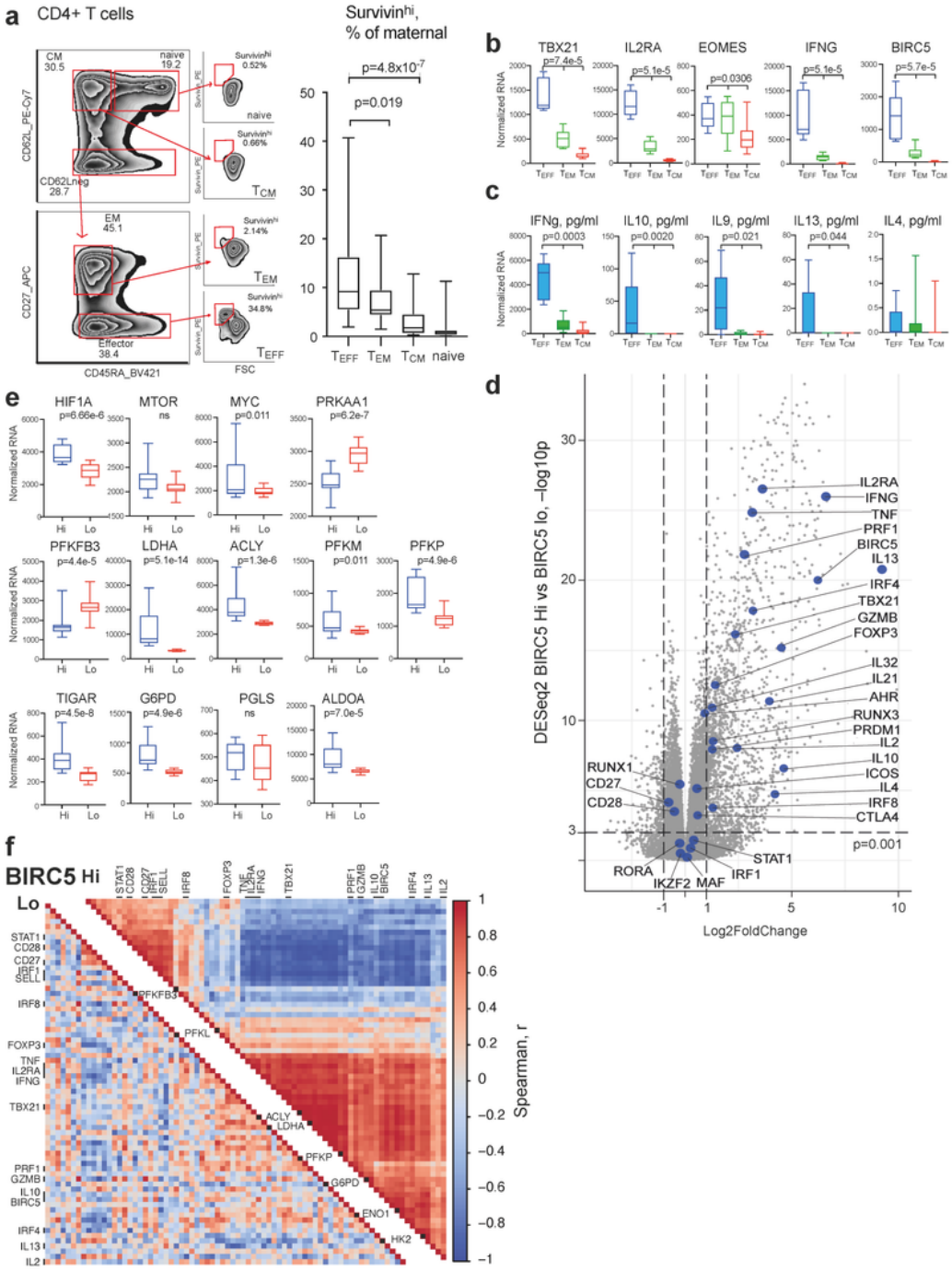

Figure 1

Survivin is essential for the phenotype of IFNg-producing CD4^{+} T cells. **a** Example of gating of naïve (CD62L^{hi}CD45RA^{+}), central memory (CM, CD62L^{hi}CD45RA^{neg}), effector memory (EM, CD62L^{neg}CD45RA^{neg}CD27^{hi}), and effector (EFF, CD62L^{neg}CD45RA$^{+/-}$CD27^{neg}) populations of survivin^{hi}CD4^{+} cells. Box plot of survivin^{hi}CD4^{+} cell frequency in 22 RA patients. *P* values were

determined by Wilcoxon test. **b,c** Box plots of gene expression analysis by RNA-seq **(b)** and cytokines by protein levels in supernatants in T_{EFF}, T_{CM}, and T_{EM} clusters of sorted $CD4^+$ cells stimulated with aCD3 for 48 h (RA patients, n=24) (**c**). *P* values were determined with DESeq2 and by Wilcoxon test. **d** Volcano plot of DE protein-coding genes in *BIRC5*^{hi} and *BIRC5*^{lo} cells. Th1 signature genes are indicated. **e** Box plots of gene RNA-seq expression analysis of metabolic regulators and glycolytic enzymes in *BIRC5*^{hi} and *BIRC5*^{lo} (median split) of $CD4^+$ cells sorted as above. *P* values were determined with DESeq2. **f** Correlation matrix of Th1 signature genes and glycolytic enzymes in *BIRC5*^{hi} and *BIRC5*^{lo} cells. Unsupervised clustering was done with corrplot Bioconductor in R-studio.

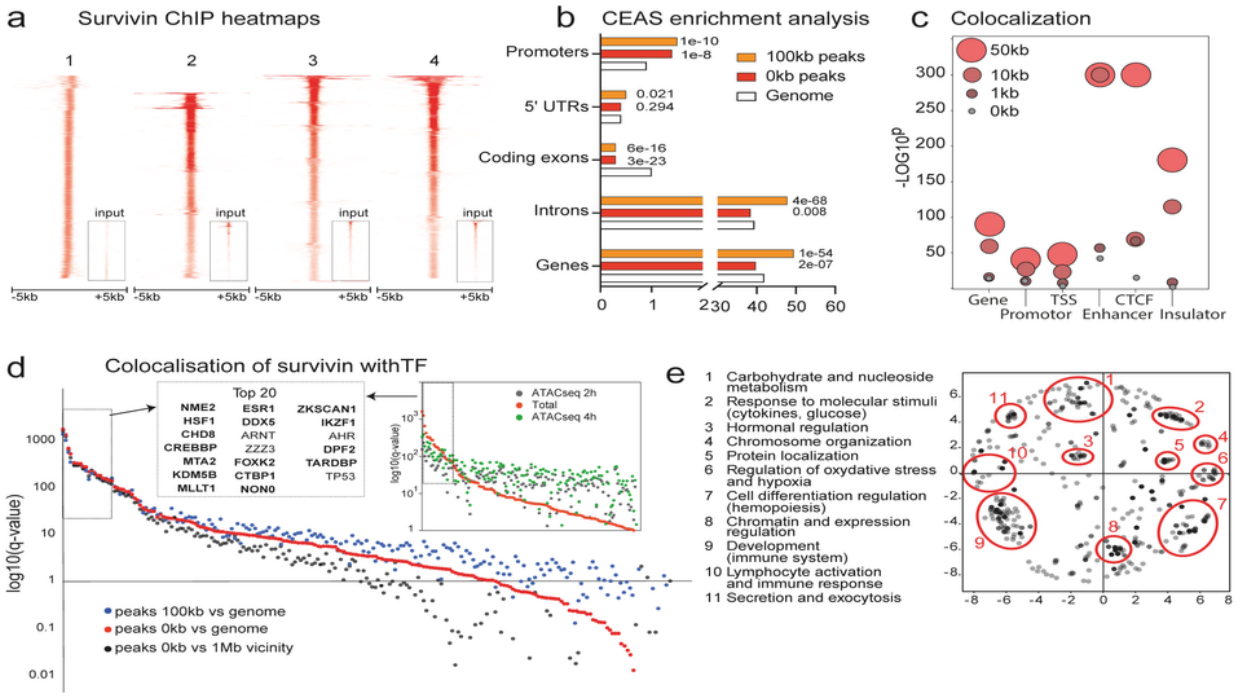

Figure 2

Binding of survivin to chromatin is predicted to regulate carbohydrate metabolism. **a** Heatmap of survivin-ChIP-seq peaks from CD4$^+$ T cells (n = 4 independent replicates). **b** Bar plots of the distribution of survivin peaks (red bars, 0-kb flanks; orange bars, 100-kb flanks) compared to the genome (open bars). **c** Dot plot of enrichment significance for colocalization of survivin peaks and DNA elements. P values were determined by two-tailed Fisher's exact test. **d** Dot plot of individual q values for colocalization of survivin

and TF ChIP-seq peaks (ReMap2020). Red dots, 0-kb flanks, 10% overlap; blue dots, 100-kb flanks; black dots, 1-Mb genome neighborhood. Only TFs with >100 events are shown. **Inset** Dot plot of q values for colocalization of TFs and survivin peaks in open chromatin regions. Common TFs are indicated in bold. **e** Semantic similarity map of Gene Ontology biological processes regulated by TFs that colocalized with survivin. Functional annotation was done in MetaScape.

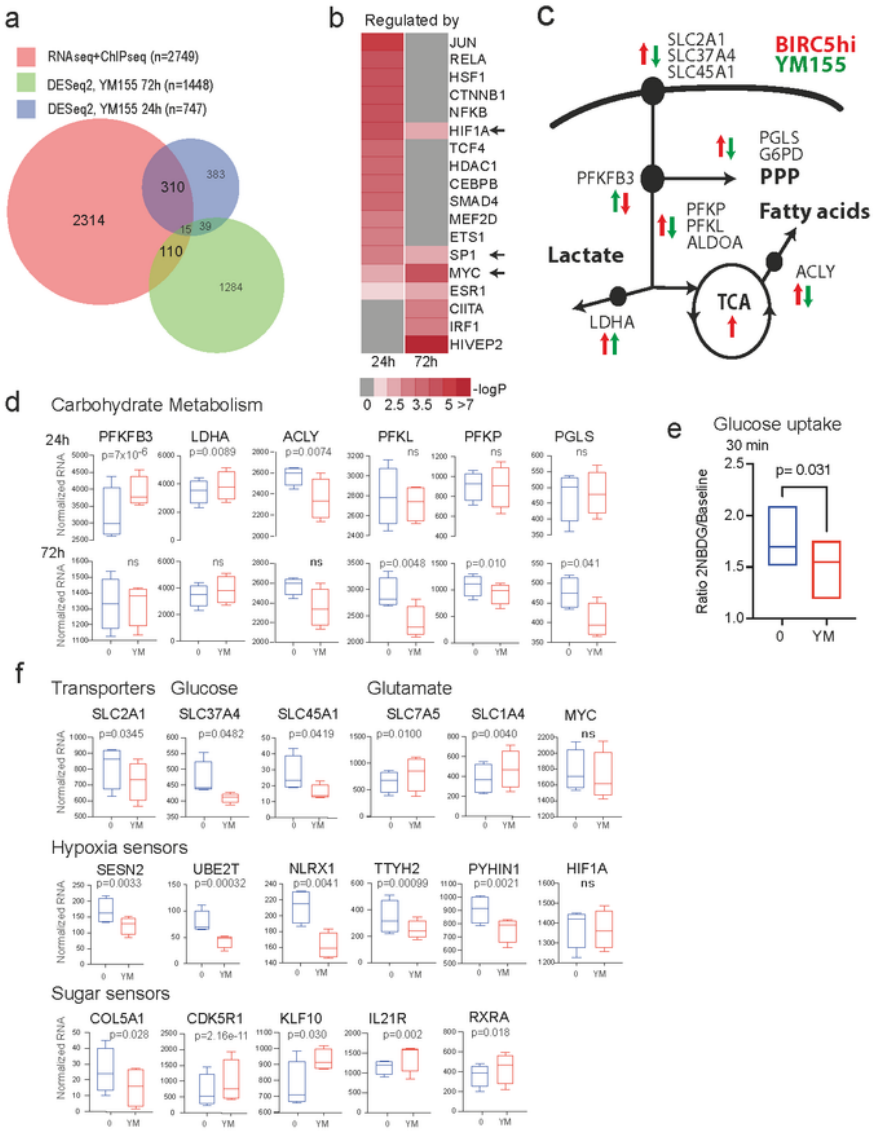

Figure 3

Figure 3

Survivin controls glycolysis through the phosphofructokinase metabolic axis. RNA-seq of $CD4^+$ T cells (n=4) treated with aCD3 and the survivin inhibitor YM155 (0 and 10 nM) for 24 or 72 h and activated with IFNg during the last 2 h. *P* values were determined with paired DESeq2. **a** Venn diagram of common protein-coding genes expressed in $CD4^+$ cells (normalized RNA value >1) and annotated to survivin peaks, and DEGs (nominal $p < 0.05$) in cells treated with YM155 for 24 or 72 h. **b** Heatmap of upstream regulators of DEGs annotated with the TRUSST database. **c.** Schematic of glucose metabolism. Arrows indicate DEGs in $BIRC5^{hi}$ cells (red) and YM155-treated cells (green). **d** Box plots of gene expression by RNA-seq of glycolytic enzymes. **e** Box plots of 2NBD-glucose uptake by YM155-treated $CD4^+$ cells, normalized to baseline. *P* values were determined by paired Wilcoxon's sign-rank test. **f** Box plots of the gene expression by RNA-seq. Nominal *p* values were determined with DESeq2.

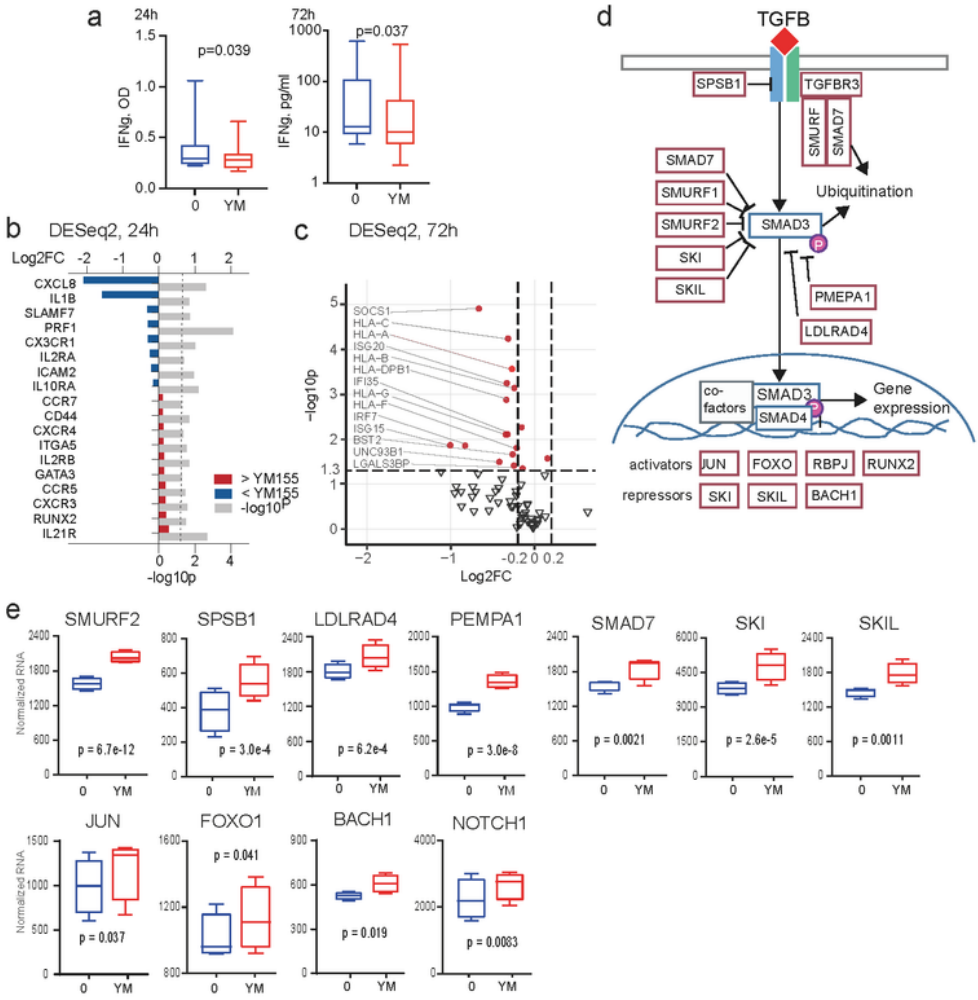

Figure 4

Inhibition of survivin activates TGFb/SMAD3 signaling. **a** CD4$^+$ T cells were activated with ConA/LPS in the presence of the survivin inhibitor YM155 (0 and 10 nM). Protein IFNg levels were measured in supernatants after 24 and 72 h. **b,c,e** RNA-seq of CD4$^+$ T cells (n = 4) treated with aCD3 and YM155 (0 and 10 nM), activated with IFNg during last 2 h. P values were determined by paired DESeq2; nominal p values are shown. **b** Forest plot of the enrichment and p values of IFN-sensitive DEGs at 24 h. **c** Volcano

plot of IFN-sensitive DEGs at 72 h. Red dots indicate clinically relevant IFN-sensitive genes. **d** Schematic of the TGFb/SMAD signaling pathway. **e** Box plots of gene expression of TGFb signalling mediators at 24 h.

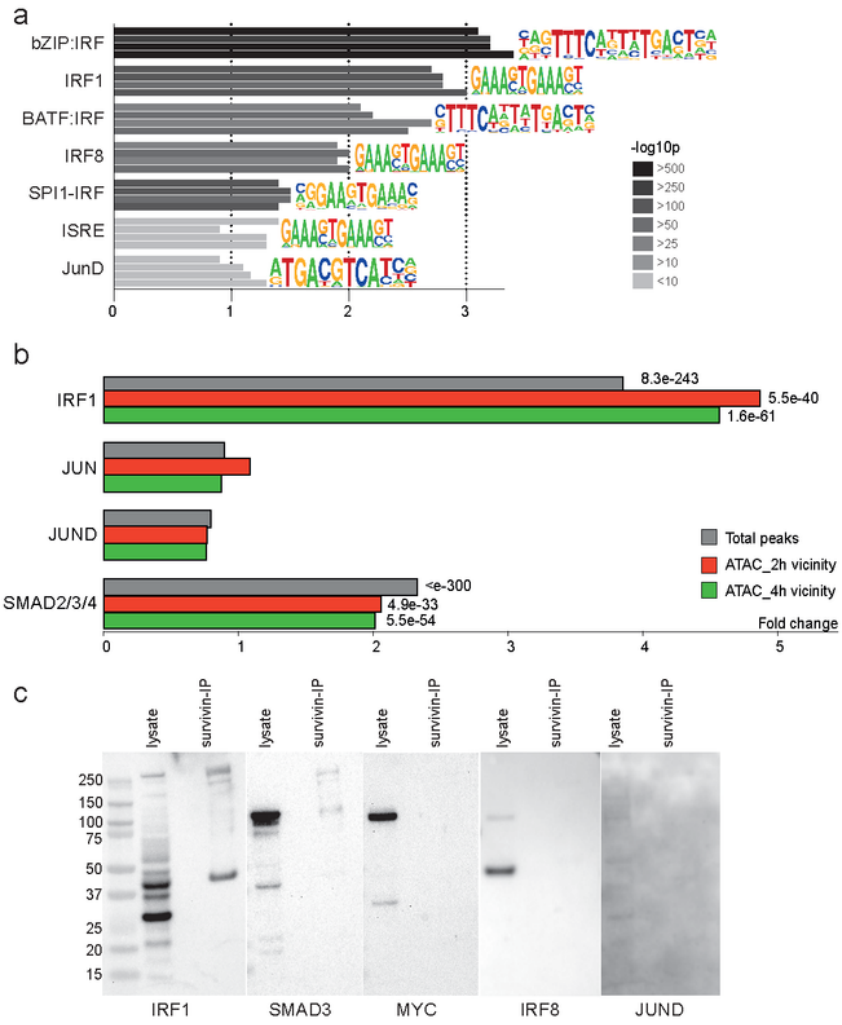

Figure 5

Survivin is recruited to chromatin by binding to IRF1 and SMAD3. **a** Bar plots of the enrichment and significance of IFNg-relevant DNA motifs identified by *de novo* motif search in nonredundant survivin-ChIP peaks (enrichment against input, corrected $p < 10^{-5}$) ($n = 4$ independent replicates), by JASPAR database. **b** Bar plots of motif enrichment in survivin peaks (0–10-kb flanks) in open chromatin regions. **c** Western blots of THP1 cell lysate before and after affinity immunoprecipitation with survivin, stained for IRF1, SMAD3, c-MYC, IRF8, and JUND.

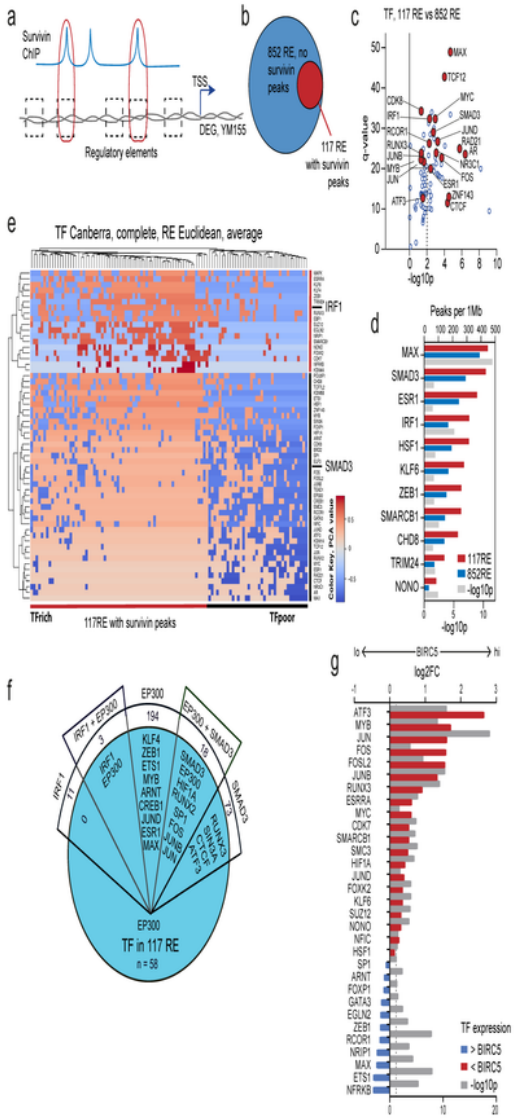

Figure 6

IRF1 and SMAD3 are predicted survivin partners in gene regulation. **a** Selection of REs paired to protein-coding DEGs. **b** Venn diagram of all REs (n=969) and survivin-containing REs (0–10-kb flanks, *n* = 117). **c** Scatter plot of TFs enriched in survivin-containing REs against remaining REs (*x*-axis, -log10 *p* value) and the genome (*y*-axis, q value). TFs in >75% of 117 REs are indicated. **d** Bar plot of TF density by ChIP-seq peaks (ReMap) in survivin-containing REs (red) and remaining REs (blue) and the significance (gray) of

differences between them. **e** Heatmap of principal component analysis of enriched TFs in individual survivin-containing REs. REs were clustered by Euclidean distance and TFs by Canberra distance. Only TFs expressed in $CD4^+$ cells (n = 58) were analyzed. **f** Protein–protein interaction by the BioGrid of IRF1, SMAD3, and EP300. **G.** Forest plot of the enrichment and p values of TFs in $BIRC5^{hi}$ versus $BIRC5^{lo}$ $CD4^+$ cells from 24 RA patients. RNA-seq data were analyzed with DESeq2.

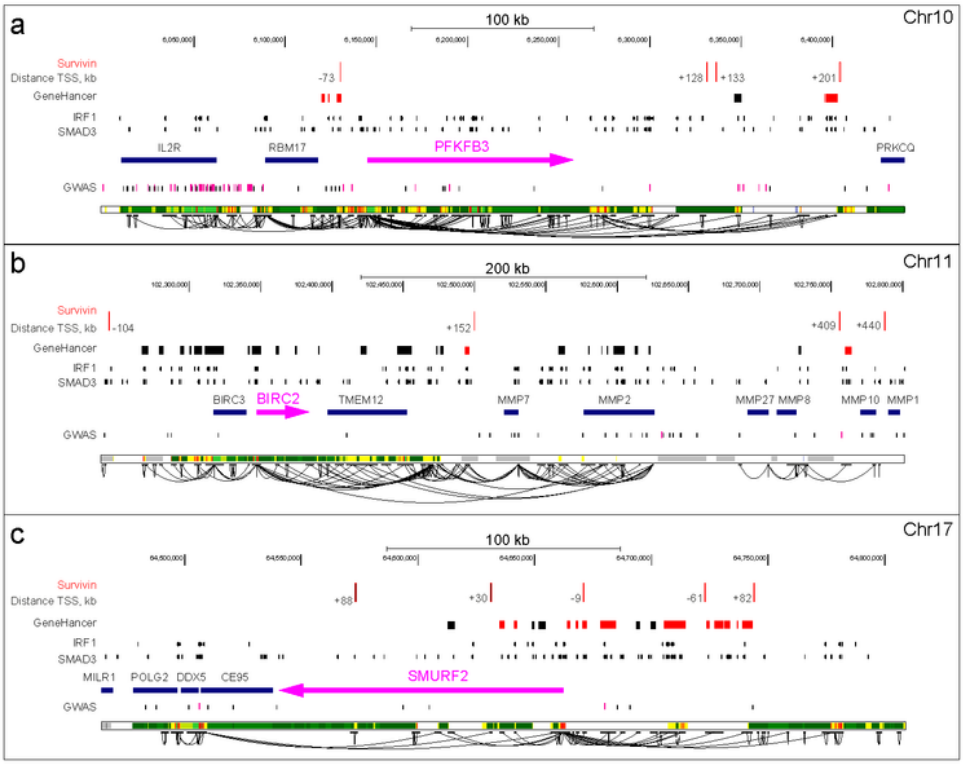

Figure 7

Figure 7

Regulatory pattern of chromatin-survivin in $CD4^+$ T cells. **a–c** Genomic maps of *PFKFB3* **(a),** *BIRC2* **(b)**, and *SMURF2* **(c)**. Magenta indicates position of the canonical gene transcript; arrow indicates transcription orientation. Red dashes at the top of each locus indicate the positions of survivin-ChIP peaks. Distances to TSSs are shown. Boxes indicate REs paired to the gene, as determined with GeneHancer. Solid curved lines indicate integrated annotation of RE connections identified with GeneHancer. Red boxes indicate REs <10 kb from the survivin peak. Vertical lines indicate positions of ChIPSeq peaks for IRF1 and SMAD3 determined by ReMap2020. Vertical lines indicate positions of GWAS SNPs associated with metabolic and autoimmune triads according to NHGRI GWAS catalog. Functional chromatin segmentation for activated $CD4^+$ cells (RoadMap ChromHMM. E042:$CD4^+CD25^-IL17^+$_PMA-Ionomyc_stimulated_Th17_Primary_Cells) is shown at the bottom of each map. Green blocks indicate actively transcribed areas; yellow blocks indicate enhancers; red blocks indicate active promoters; gray blocks indicate areas of repressed (dark gray) and poised (light gray) chromatin.

Supplementary Files

This is a list of supplementary files associated with this preprint. Click to download.

- supplFigure1Erlandsson.ai
- supplFigure2Erlandsson.ai
- supplFigure3Erlandsson.ai
- supplFigure4Erlandsson.ai
- supplFigure5Erlandsson.ai
- SupplementaryTables.docx